Interferometry Based Integrated Sensing and Communications with Imperfect Synchronizations

Terry N. Guo, Allen B. MacKenzie and Husheng Li

***Abstract*—Interferometry is a powerful tool for estimating the incident angle of electromagnetic (EM) waves by calculating the correlation of received signals at different antennas. Motivated by very-long-baseline interfereometry (VLBI) in radio astronomy, an interferometry based sensing scheme is proposed as integrated sensing and communications (ISAC). It reuses the communication signal from base stations (BSs), similarly to passive radars, which improves the sensing precision and spectrum efficiency. Different from the almost-perfect synchronization in VLBI realized by atomic clocks, the synchronization in BSs of cellular communication networks (usually based on GPS signals) could have significant errors. Therefore, algorithms for compensating for synchronization errors in both time and frequency are proposed. Numerical simulations demonstrate that the proposed algorithms can substantially alleviate the synchronization errors.**

***Index Terms*—Interferometry, synchronization, integrated sensing and communications, passive radar**

I. Introduction

There is a long history of reusing communication signals for radar sensing (as a passive radar), in which the illumination by communication signal is not originally intended for radar sensing, thus being a 'bonus' brought by communications. Essentially this technique is a prospective candidate for integrated sensing and communications (ISAC) [1]. An early example dates back to 1935, when R. Waston detected an aircraft by using reflected waves originated from a short-wave radio station in UK [2]. Nowadays, Wi-Fi signals have been intensively used for sensing, such as gesture detection, target monitoring, and sleep surveillance [3], [4]. Meanwhile, cellular communication networks have been used for target positioning. The performance has been substantially improved since the deployment of 5G cellular networks; e.g., precisions of up to 3m (vertical and horizontal, indoors) and 10m (horizontal, outdoors) have been attained in 3GPP TR 38.857 [5], while an indoor positioning experiment by Qualcomm has achieved a precision of 30cm [6].

Although substantial progress has been made for communication-signal-based sensing, existing schemes face various limitations: (a) When machine learning is employed for sensing, such as in many Wi-Fi-based sensing schemes, a change of environment may cause an outage for the learned classifier. (b) The size of antenna array limits the angular resolution, which is proportional to λ/D, namely the ratio between wavelength λ and aperture radius D. To improve the sensing precision, with robustness to environment change, a novel mechanism of sensing is urgently need. We are motivated by a milestone achievement in radio astronomy, namely the first successful imaging of black hole in 2019 [7]. The black hole is 550 light years away from the earth, thus requiring an angular resolution of 20 microarcseconds. The technique used 8 radio astronomy telescopes distributed over the earth (ranging from Antarctic to Spain). In particular, the system works in the millimeter wave (mmWave) band with wavelength 1 mm, which is relatively close to the mmWave bands of 5G communication systems. The key technique in imaging the black hole is very-long-baseline interferometry (VLBI) [8], which leverages the high sensitivity of interferometry of EM waves to target displacement.

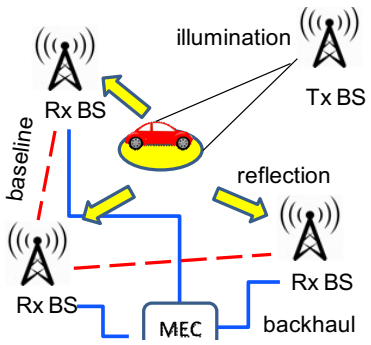

Fig. 1: Interferometry-based ISAC

Thanks to the dense deployment of 5G base stations (BSs), we propose to employ the technique of VLBI for fine sensing in ISAC (not necessarily in the mmWave band) in outdoor scenarios[1]. As illustrated in Fig. 1, the BSs form many baselines (namely the line between two BSs) for sensing. When a communication signal beam from a transmit BS illuminates a certain area (e.g., the area around a receiving user equipment (UE)), the reflected signals are received by multiple BSs and then delivered to a center (e.g., the multiaccess edge computing (MEC)) for analysis, based on the principle of interferometry. Various applications are expected for the proposed sensing scheme, such as outdoor positioning and vehicle surveillance. The detailed algorithm has been described in [9]. This paper will mainly address the practical challenges in the interferometry based ISAC.

T. N. Guo is with the Center for Manufacturing Research, Tennessee Technological University, Cookeville, TN (email: nguo@tntech.edu). A. B. MacKenzie is with the Dept. of Electrical and Computer Engineering, Tennessee Technological University, Cookeville, TN (email: amackenzie@tntech.edu). H. Li is with the Department of Electrical Engineering and Computer Science, the University of Tennessee, Knoxville, TN (email: hli31@utk.edu).

[1]For indoor scenarios, it is still unclear whether the interferometry approach is valid, due to the large number of propagation paths.

A major challenge to interferometry based sensing is the time synchronization error at different BSs: (a) Time synchronization: In radio astronomy, atomic clocks are used for the black hole imaging. However, atomic clocks are too expensive to use in 5G systems, which achieve time synchronization of BSs by GPS or IEEE1588-2019. When the total timing error contributed by the GPS and infrastructure circuits is significant, this becomes a key challenge and compensation techniques are needed. (b) Frequency synchronization: The received signals at different BSs are down-converted to the baseband and sent for computing. The frequency offset of local oscillators (for the frequency down-conversion) will have a significant impact on the sensing precision. Therefore, we will address interferometry based ISAC with imperfect synchronization. On the one hand, we will develop an autofocus algorithm to reduce the time synchronization error without a reference signal; on the other hand, we will estimate the frequency offset of local oscillators and compensate for it in the sensing results. Both approaches will be demonstrated using numerical simulations.

This paper is organized as follows. The related work is introduced in Section II. The system model, including the system architecture, signaling, and interferometry, is introduced in Section III. Then, algorithms to mitigate the time and frequency synchronization errors are proposed in Section IV and V, respectively. The numerical results and conclusions are provided in Sections VI and VII, respectively.

II. Related Works

5G signals have been expected to achieve precise positioning of UEs, as explained in the introduction [5], [6]. In the mmWave band, the communication signal can be used for localization, based on different signal features [10]. In [11], the possibility of embedding sensing function (e.g., as the preamble of OFDM symbol) in communication signals has been analyzed. In [12], a 60 GHz radio signal is used for target tracking, which is similar to a bi-static radio system. The angle of arrival (AOA) of a mmWave signal is studied in [13], which can be used for positioning. Essentially, the proposed sensing scheme is related to passive bistatic radars [14], in which the radar leverages other radiation sources [2]. The exogenous radiation source could be an OFDM TV broadcast [15], a GPS signal [16], or an LTE signal [17].

Interferometry is widely used for imaging in the optical frequency band [18]. For the radio frequency (RF) domain, the most significant application is the VLBI imaging in radio astronomy [19]. There has also been a long history of employing phase interferometry in AOA estimation [20]. Although these algorithms also use interferometry by calculating the correlation, the traditional phase interferometry does not add intentional delay to the signal and estimates the AOA by estimating the phase difference in the signals. Therefore, phase interferometry is valid for far field narrow band signals, with large wavelength and short baseline distance.

III. System Model

In this section, we introduce the system model of the interferometry based ISAC.

A. System Architecture

For practical 5G cellular systems, we consider the finer structure within one BS in this paper, in which each BS consists of two major units: Remote Radio Unit (RRU) and Baseband Unit (BBU). The RRUs are connected to the BBU via front hauls, using the Common Public Radio Interface (CPRI) standard [21], [22]. BBUs of different BSs are further connected to the core network via backhauls. For the proposed interferometry based ISAC, multiple antenna arrays at separated RRUs form interferometry baselines. The signals received at the RRUs are down-converted to baseband IQ data and then transmitted to the BBU via CPRI links. Then the interferometry (namely the calculation of correlation function) in the baseband is performed at the BBU. In this paper, we focus on a single BBU with multiple RRUs. The study can be easily extended to the case of multiple BBUs.

B. Signal Model

Consider two antennas with baseline length (distance) D, and a planar EM wave having incident angle θ, radian frequency ω, and wavenumber $k = \frac{\omega}{c}$ (where c is the speed of light). The received signals at the two antennas are denoted by $S_1(t)$ and $S_2(t)$, respectively. Suppose that the signal arrives at antenna 1 first. Then we have

$$S_2(t) = S_1(t)e^{-j\omega t - jkD\cos\theta}, \tag{1}$$

which discloses the phase difference between S_1 and S_2 due to the baseline length. The single-tone signal model can be easily extended to wideband signals (omitted due to space limitations).

C. Interferometry

In interferometry, the incident angle is obtained from the correlation function between S_1 and S_2, namely

$$R(\tau) = \int_{\mathbb{R}} S_1(t)S_2(t-\tau)dt, \tag{2}$$

where τ is the artificial delay added to S_2. We notice that when $\tau = \frac{D\cos\theta}{c}$, S_1 and S_2 are in-phase and thus result in a peak in the correlation function R. The peak time τ is then used as the estimation of the time difference of arrival (TDOA), based on which the AOA θ is estimated. Note that, for single-tone signals, the correlation function $R(\tau)$ is periodic, with period $\frac{2\pi}{\omega}$. To remove the ambiguity, we leverage the following two possible redundancies:

- Multiple tones: In wideband communication signals with multiple subcarriers, the correlation function will become peaky and thus remove the ambiguity.
- Multiple baselines: When there are more than one baselines, the AOA estimations at different baselines should be consistent, thus eliminating the ambiguity.

The details of using multiple tones or baselines for eliminating the ambiguity are omitted due to limited space.

IV. Autofocus for Combating Timing Error

In the calculation of correlation for interferometry in (2), we assume that S_1 and S_2 have the same timing. However, this is prohibitively difficult, due to the imperfection of timing source (e.g., the GPS signal). Therefore, when there is a timing offset $\Delta\tau$, the resulting correlation function is actually given by

$$R(\tau) = \int_{\mathbb{R}} S_1(t) S_2(t - \Delta\tau - \tau) dt, \tag{3}$$

which introduces an error $\Delta\theta \approx -\frac{c\Delta\tau}{\sqrt{D^2-(\tau c)^2}}$.

When there is a single baseline, it is impossible to identify the timing error and thus the error in the AOA estimate. Therefore, we seek help from multiple baselines. The principle is that the outcomes of the AOA estimates of different baselines need to be consistent. In this paper, we consider N receiving BSs (thus $Q = \frac{N(N-1)}{2}$ baselines). BS 1 is set as the reference one and the time offsets at the remaining BSs are denoted by $\Delta\tau_2$, ..., $\Delta\tau_N$. Essentially this is the procedure of autofocus, since the timing error results in the loss of focus. In the subsequent discussion, we consider the cases of a single incident wave and two incident waves, respectively.

A. Single Incident Wave

We first consider the case of a single incident wave for the autofocus algorithm, which is formulated as the following optimization problem:

$$\min_{\Delta\tau_2,\ldots,\Delta\tau_N} \sum_{i<j,m<n,(i,j)\neq(m,n)} \left[(\tau_{ij} + \Delta\tau_i - \Delta\tau_j) - (\tau_{mn} + \Delta\tau_m - \Delta\tau_n)\right]^2, \tag{4}$$

where τ_{ij} is the TDOA of BSs i and j after the corrections of baseline directions. The optimization is to minimize the disparities of incident angle cosines (instead of the angles, for a quadratic objective function) by shifting the timings. This objective function can be easily optimized by solving the linear equations resulting from the derivative. Take the simple case of $N = 3$ (i.e., three BSs and three baselines); it is easy to verify that the solution is given by

$$\begin{pmatrix} 2 & -3 & 1 \\ 1 & -2 & 1 \\ 1 & -3 & 2 \end{pmatrix} \begin{pmatrix} \Delta\tau_1 \\ \Delta\tau_2 \\ \Delta\tau_3 \end{pmatrix} = \begin{pmatrix} 2\tau_{23} - \tau_{12} - \tau_{13} \\ \tau_{23} - \tau_{12} \\ \tau_{13} + \tau_{23} - 2\tau_{12}) \end{pmatrix} \tag{5}$$

where we set $\Delta\tau_1 = 0$ since BS1 is the reference point. Then, $\Delta\tau_2$ and $\Delta\tau_3$ can be easily solved from the equation.

B. Double Incident Waves

Now we consider the case of two incident waves, such that a cross-check can be used for the autofocus (see Fig. 2), by leveraging the fact that the time synchronization error is independent of the incident waves. For simplicity, we assume that all the Q baselines have the same length D, and each suffers a constant system timing error $\Delta\tau_q$. Again, one of the baselines serves as the geometric reference, and the angle between baseline q and the reference baseline is α_q. Corresponding to a pair of true AOAs (θ, θ') of incident waves, baseline q generates a pair of AOA estimates $(\widehat{\theta}_q, \widehat{\theta'}_q)$,

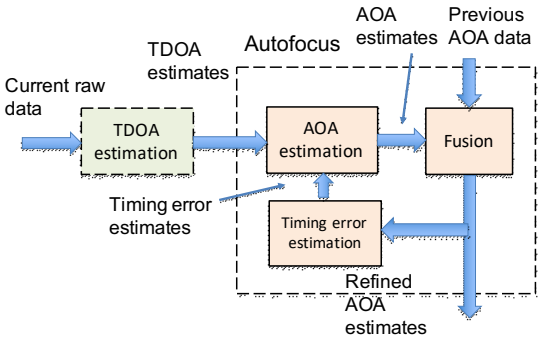

Fig. 2: Autofocus algorithm with double incident waves

$q = 1, 2, \cdots Q$. Under the far-field condition, the AOA and TDOA at baseline q are related by $\sin(\theta + \alpha_q) = \frac{c}{D}\tau_q$, where θ is the AOA with respect to the reference baseline, D is the baseline length and τ_q is the TDOA. Based on this relation, we obtain

$$\frac{d\theta}{d\tau_q} = \frac{c}{D\cos(\theta + \alpha_q)}, \tag{6}$$

which implies $\Delta\tau_q \approx (\widehat{\theta}_q - \theta)\frac{D}{c}\cos(\theta+\alpha_q)$, and $\Delta\tau_q \approx (\widehat{\theta'}_q - \theta'_p)\frac{D}{c}\cos(\theta' + \alpha_q)$. Essentially (6) expresses the sensitivity of TDOA to AOA. Define $r_q(\theta) \triangleq \frac{D}{c}\cos(\theta + \alpha_q)$. Then, we define the timing square error inversely obtained from the incident wave angle estimates as

$$\left[(\widehat{\theta}_q - \theta) r_q(\theta) - (\widehat{\theta'}_q - \theta') r_q(\theta')\right]^2, \tag{7}$$

for $q = 1, 2, \cdots, Q$. We replace $r_q(\theta)$ and $r_q(\theta')$, which are unavailable due to the unknown incident angles, with the estimates $r_q(\widehat{\theta})$ and $r_q(\widehat{\theta'})$. We denote the unknowns θ and θ' by x and x', which are estimated by minimizing the following mean square errors:

$$\min_{x,x'} \sum_{q=1}^{Q} \left[(\widehat{\theta}_q - x) r_q(\widehat{\theta}) - (\widehat{\theta'}_q - x') r_q(\widehat{\theta'})\right]^2, \tag{8}$$

where $\widehat{\theta}$ and $\widehat{\theta'}$ are given by

$$\widehat{\theta} = \frac{1}{Q}\sum_{q=1}^{Q} \widehat{\theta}_q, \ \widehat{\theta'} = \frac{1}{Q}\sum_{q=1}^{Q} \widehat{\theta'}_q. \tag{9}$$

From (8), one can solve the following equations for the least-square-error solution:

$$\begin{aligned} r_q^2(\widehat{\theta}) x - r_q(\widehat{\theta}) r_q(\widehat{\theta'}) x' &= r_q(\widehat{\theta}) \left[\widehat{\theta}_q r_q(\widehat{\theta}) - \widehat{\theta'}_q r_q(\widehat{\theta'})\right], \\ r_q(\widehat{\theta}) r_q(\widehat{\theta'}) x - r_q^2(\widehat{\theta'}) x' &= r_q(\widehat{\theta'}) \left[\widehat{\theta}_q r_q(\widehat{\theta}) - \widehat{\theta'}_q r_q(\widehat{\theta'})\right], \end{aligned} \tag{10}$$

for $q = 1, 2, 3, \cdots, Q$. The above equations can be rewritten in the following matrix form:

$$A\boldsymbol{x} = \boldsymbol{b}, \tag{11}$$

where $\boldsymbol{x} = (x, x')^T$, A is a $2Q \times 2$ matrix, and $\boldsymbol{b}$ is a $2Q$-vector, given by

$$A = \begin{pmatrix} r_1^2(\widehat{\theta}) & -r_1(\widehat{\theta}) r_1(\widehat{\theta'}) \\ r_1(\widehat{\theta}) r_1(\widehat{\theta'}) & -r_1^2(\widehat{\theta'}) \\ \vdots & \vdots \\ r_Q^2(\widehat{\theta}) & -r_Q(\widehat{\theta}) r_Q(\widehat{\theta'}) \\ r_Q(\widehat{\theta_p}) r_Q(\widehat{\theta'}) & -r_Q^2(\widehat{\theta'}) \end{pmatrix}, \tag{12}$$

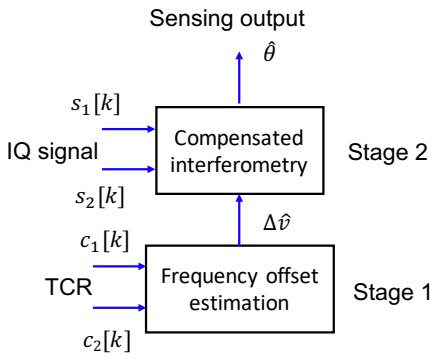

Fig. 3: The two-stage scheme for mitigating asynchronicity.

$$\boldsymbol{b}=\begin{pmatrix} r_1(\widehat{\theta})\left[\widehat{\theta}_1 r_1(\widehat{\theta})-\widehat{\theta'}_q r_q(\widehat{\theta'})\right] \\ r_1(\widehat{\theta'})\left[\widehat{\theta}_1 r_1(\widehat{\theta})-\widehat{\theta'}_1 r_1(\widehat{\theta'})\right] \\ \vdots \\ r_Q(\widehat{\theta})\left[\widehat{\theta}_Q r_Q(\widehat{\theta})-\widehat{\theta'}_Q r_Q(\widehat{\theta'})\right] \\ r_Q(\widehat{\theta'})\left[\widehat{\theta}_Q r_Q(\widehat{\theta})-\widehat{\theta'}_Q r_Q(\widehat{\theta'})\right] \end{pmatrix}. \tag{13}$$

The optimal solution is given by the generalized inversion:

$$\widehat{\boldsymbol{x}}=\left(A^T A\right)^{-1} A^T \boldsymbol{b}. \tag{14}$$

This solution also serves as the fusion algorithm for a pair of AOAs estimated by Q baselines. We further estimate the system timing errors $\Delta\tau_q$'s by using

$$\Delta\widehat{\tau}_q \triangleq \frac{1}{2}\left[(\widehat{\theta}_q - x)r_q(x)+(\widehat{\theta'}_q - x')r_q(x')\right]. \tag{15}$$

Since the system timing errors are stable, once $\Delta\widehat{\tau}_q$'s are obtained, we can reuse them to compensate the measured TDOAs in estimating any AOAs. In particular, it is possible to run timing compensation and data fusion recursively to further refine the estimates. The data fusion for a single AOA can simply be averaging over all baselines (see Eq. (9)).

V. Compensation of Frequency Mismatches

An alternative significant concern in the interferometry based ISAC is the mismatch of local oscillators (LOs). Because the RRUs do not share a common LO or use atomic clocks like Hydrogen maser [23], [24], for the frequency down-conversion and sampling, the baseband IQ data streams from the RRUs contain unknown intrinsic phases, due to the frequency mismatch in the RRU LOs. In the proposed system, to handle the frequency mismatch, we propose to use a transmitted clock reference (TCR) which can be transmitted periodically at a low duty cycle, as well as a two-stage approach illustrated in Fig. 3.

A. Stage 1. Frequency Offset Estimation

To start with, consider a simple case of two RRUs and a passband signal with center frequency ω_0, for notational simplicity, which will be extended to more sophisticated scenarios. Assume that the passband signal has sufficient large bandwidth and peaky autocorrelation. The LO frequencies and sampling intervals of the two RRUs are ω_i and $T_{S,i}$, $i = 1, 2$, respectively, while the nominal frequency and sampling interval are ω and T_S, respectively. Thermal noise, as well as frequency and time jitters, are temporarily omitted due to their minor impacts. Since the LOs at different RRUs are not perfectly aligned, one introduces $\Delta\omega_i$, the LO frequency error for RRU$_i$, $i = 1, 2$, or the illuminating source ($i = 0$), with respect to the nominal value ω, i.e., $\omega_i = \omega + \Delta\omega_i$, $i = 0, 1, 2$. Let $\Delta T_{S,i}$ be the sampling interval error for RRU$_i$, $i = 1, 2$, or the illuminating source ($i = 0$), with respect to the nominal value T_S; i.e., $T_{S,i} = T_S + \Delta T_{S,i}$, $i = 0, 1, 2$. Because $T_S \propto 1/\omega$ or $\omega T_S = constant$, one has $\frac{\Delta T_{S,i}}{T_S} = \omega\left[\frac{1}{\omega+\Delta\omega_i} - \frac{1}{\omega}\right] = \frac{-\Delta\omega_i}{\omega+\Delta\omega_i} \approx \frac{-\Delta\omega_i}{\omega}$. These ratios are bounded by the LO accuracy in parts per million (PPM). After the frequency down-conversion, the received signal at RRU$_i$, $i = 1, 2$, is converted to an IQ data stream. Omitting the attenuation due to reflection, the IQ data is given by

$$\begin{aligned} S_i[k] &= a\left(kT_{S,i}+\Delta t_i\right)e^{j[(\Omega_D+\omega_0-\omega_i)kT_{S,i}+\phi_i+\psi_i)]} \\ &= a(k(T_S+\Delta T_{S,i})+\Delta t_i) \\ &\quad\times\quad e^{j[(\Omega_D+\Delta\omega_0-\Delta\omega_i)k(T_S+\Delta T_{S,i})+\phi_i+\psi_i]} \\ &\triangleq a(k(T_S+\Delta T_{S,i})+\Delta t_i)e^{j[\xi_i k(T_S+\Delta T_{S,i})+\phi_i+\psi_i]} \\ &\approx a(k(T_S+\Delta T_{S,i})+\Delta t_i)e^{j[kT_S\xi_i+\phi_i+\psi_i]}, \end{aligned} \tag{16}$$

where $\xi_i \triangleq \Omega_D + \Delta\omega_0 - \Delta\omega_i$, for $k = 1, 2, \cdots$. where $a(\cdot)$ is the sample of complex envelope, k is the time index, Δt_i is an unknown time lag, Ω_D is the Doppler frequency, $\xi_i \triangleq \Omega_D + \Delta\omega_0 - \Delta\omega_i$ is the unknown frequency error due to Doppler shift and frequency drift, ϕ_i is the phase corresponding to signal travel time, and ψ_i is the unknown initial phase at LO i, introduced during the quadrature down-conversion.

The TCR is encoded in the IQ format (this complex-value TCR can simply come from the orthogonal LO pair $\{\cos(\cdot)$ and $\sin(\cdot)\}$ used for quadrature down-conversion), which is given by

$$c_i[k] = e^{j(\omega_i kT_{S,i}+\overline{\psi}_i)} \triangleq e^{j(kT_S\omega+\overline{\psi}_i)}e^{jkT_S\nu_i} \tag{17}$$

where $\overline{\psi}_i$ is an unknown phase similar to ψ_i, and $\nu_i \triangleq \Delta\omega_i + (\omega+\Delta\omega_i)\Delta T_{S,i}/T_S$ is the comprehensive unknown frequency drift due to the LO frequency error. It will be explained in the subsequent discussion that the correlation function for interferometry is perturbed by a time-varying term close to $e^{-jkT_S\Delta\nu_i/2}$, which needs to be canceled in the computation of correlation. Hence, $\Delta\nu \triangleq \nu_2 - \nu_1$, namely the offset of the two frequency drifts, should be estimated for the compensation procedure. In this paper, we use the estimation procedure illustrated in Fig. 4. The detailed derivation is omitted due to the limited space.

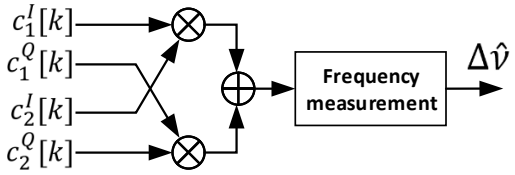

Fig. 4: Estimating $\Delta\nu$.

B. Stage 2. Compensating Frequency Offset

The TDOA τ can be estimated by calculating the correlation between the two IQ signal $S_1[k]$ and $S_2[k]$, namely

$$\begin{aligned} R[m] &= \frac{1}{W}\sum_{k=n_0}^{n_0+W-1} S_1^*[k-m]S_2[k] \\ &= e^{j[mT_S(1+\Delta T_{S,1}/T_S)\xi_1+\phi_2-\phi_1+\psi_2-\psi_1]} \\ &\times \frac{1}{W}\sum_{k=n_0}^{n_0+W-1} a^*((k-m)(T_S+\Delta T_{S,1})+\Delta t_1) \\ &\times a(k(T_S+\Delta T_{S,2})+\Delta t_2)\cdot e^{jkT_S\beta}, \end{aligned} \tag{18}$$

where the factor β is defined as

$$\begin{aligned} \beta &\triangleq [(\Omega_D+\Delta\omega_0)(\Delta T_{S,2}-\Delta T_{S,1}) \\ &+ \Delta\omega_1\Delta T_{S,1}-\Delta\omega_2\Delta T_{S,2}]/T_S-(\Delta\omega_2-\Delta\omega_1) \\ &\approx (\Omega_D+\Delta\omega_0)(\Delta T_{S,2}-\Delta T_{S,1})/T_S-(\Delta\omega_2-\Delta\omega_1), \end{aligned} \tag{19}$$

and W is the correlation window size. Then, the TDOA estimate $\widehat{\tau}$ can be obtained using $\widehat{m}=\arg\max_m |R[m]|$ and $\widehat{\tau}=\widehat{m}T_S$.

It is worth noting that in (19) β is an undesired frequency dominated by $\pm|\Delta\omega_2-\Delta\omega_1|$. In the worst case β is in the order of $2\times ppm\times\omega$ corresponding to 1.2 MHz for $ppm=10\times10^{-6}$ and center frequency 60 GHz. Fortunately, this undesired frequency can be significantly reduced with $\Delta\widehat{\nu}$. By using approximation $\Delta T_{S,i}/T_S\approx\Delta\omega_i/\omega$, one has

$$\begin{aligned} \Delta\nu &= \Delta\omega_2+(\omega+\Delta\omega_2)\Delta T_{S,2}/T_S \\ &- \Delta\omega_1-(\omega+\Delta\omega_1)\Delta T_{S,1}/T_S \\ &= (\Delta\omega_2-\Delta\omega_1) \\ &+ \frac{1}{T_S}[\omega(\Delta T_{S,2}-\Delta T_{S,1})+\Delta T_{S,2}\Delta\omega_2-\Delta T_{S,1}\Delta\omega_1] \\ &\approx (\Delta\omega_2-\Delta\omega_1)+\frac{1}{T_S}[\omega(\Delta T_{S,2}-\Delta T_{S,1})] \\ &\approx 2(\Delta\omega_2-\Delta\omega_1). \end{aligned} \tag{20}$$

Therefore, by using a phase rotating term $e^{jkT_S\Delta\widehat{\nu}/2}$, the compensated correlation is given by

$$\begin{aligned} R[m] &= \frac{1}{W}\sum_{k=n_0}^{n_0+W-1} S_1^*[k-m]S_2[k]e^{jkT_S\Delta\widehat{\nu}/2} \\ &= e^{j[mT_S(1+\Delta T_{S,1}/T_S)\xi_1+\phi_2-\phi_1+\psi_2-\psi_1]} \\ &\times \frac{1}{W}\sum_{k=n_0}^{n_0+W-1} a^*((k-m)(T_S+\Delta T_{S,1})+\Delta t_1) \\ &\times a(k(T_S+\Delta T_{S,2})+\Delta t_2)\cdot e^{jkT_S\beta'}, \end{aligned} \tag{21}$$

where the factor β' is defined as

$$\begin{aligned} \beta' &\triangleq [(\Omega_D+\Delta\omega_0)(\Delta T_{S,2}-\Delta T_{S,1}) \\ &+ \Delta\omega_1\Delta T_{S,1}-\Delta\omega_2\Delta T_{S,2}]/T_S \\ &- (\Delta\omega_2-\Delta\omega_1)+\Delta\widehat{\nu}/2 \\ &\approx (\Omega_D+\Delta\omega_0)(\Delta T_{S,2}-\Delta T_{S,1})/T_S, \end{aligned} \tag{22}$$

where the approximation $\Delta\widehat{\nu}/2\approx\Delta\nu/2\approx\Delta\omega_2-\Delta\omega_1$ has been applied. Eventually, the undesired frequency is significantly reduced from β to β'.

VI. Numerical Results

In this section, we provide numerical results to demonstrate the proposed algorithms.

A. Impact of Errors and System Numerology

Based on the sensitivity in (6), a TDOA estimation error $\Delta\tau$ roughly leads to an AOA estimation error $\frac{\Delta\tau c}{D\cos(\theta)}$. The PPS accuracy is in nanoseconds [25]. The AOA estimation error is about 1.72° for $\Delta\tau=5$ ns, $D=100$ meters and $\theta=60^\circ$. The same sensitivity formula can be used in selecting the sampling interval T_S. The time resolution of the correlator is $T_S/2$, corresponding to an AOA estimation resolution $\frac{T_S c}{2D\cos(\theta)}$.

The correlator length W is the processing gain that has to be large enough to suppresse the noise impact. However, an increasing W can lead to an accumulated time offset $W|\Delta T_{S,2}-\Delta T_{S,1}|$ which can be $2ppmWT_S$ in the worst case. Roughly speaking, the width of the correlation peak is in the same order of the inverse of the signal bandwidth B. One can have the following thumb rule as a constraint on the correlation length: $2ppmWT_S<1/B$, or equivalently, $W<\frac{1}{2ppmT_SB}$ which is 5×10^4 for $ppm=10\times10^{-6}$, $T_S=2$ ns and $B=500$ MHz.

B. Autofocus

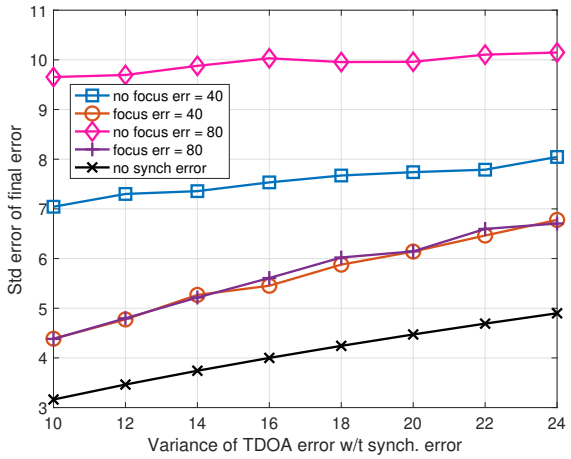

Fig. 5: MSE of autofocus error with a single incident wave

For the single incident wave case, the simulation results for $Q=3$ are shown in Fig. 5, where the time unit is the sampling period T_s. We observe that the TDOA error can be substantially reduced, while it cannot be completely removed when compared with the case of no timing error.

For the case of two incident waves, we have tested the method in (14) using simulations. We consider three 100-meter baselines set with angles of 0°, -15° and 15° with respect to the reference baseline. The simulated AOA estimation errors in RMS are shown in Fig. 6 for AOA between -60° and 60°, based on previous data for a pair of AOAs -45° and 45°, assuming the ensemble of system timing errors ($\Delta\tau$) under test follows a zero-mean normal distribution.

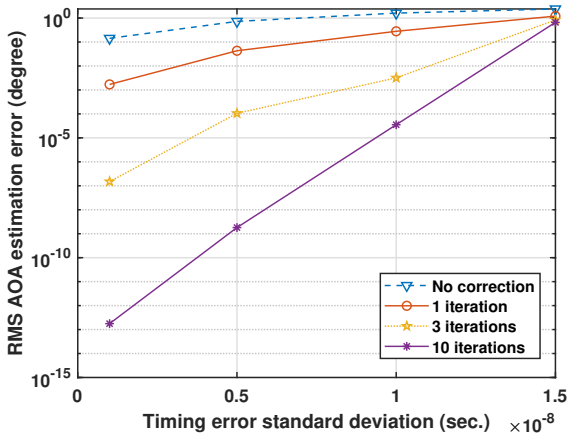

Fig. 6: AOA estimation errors vs. timing errors.

TABLE I: Worst-case results for clock error compensation.

ppm $(\times 10^{-6})$		0	1	5	10
Without compensation	Peak	0.976	0.069	0.064	0.060
	Location	0	-208	-692	-1411
With 95% compensation	Peak	0.976	0.961	0.678	0.113
	Location	0	0	0	0
With full compensation	Peak	0.976	0.976	0.976	0.976
	Location	0	0	0	0

C. Compensation of Frequency Errors

For the simulation on frequency error compensation, the parameters are set as follows: signal bandwidth 200 MHz, sampling frequency 500 MHz, correlation length $W = 7,500$, and SNR=0 dB. The numerical results for the worst case (i.e., $|\Delta T_{S,2} - \Delta T_{S,1}|/T_S \approx |\Delta\omega_2 - \Delta\omega_1|/\omega = 2ppm$) are provided in Table I, where the correlation peak value is normalized, the peak location is the offset with respect to the desired value and measured in samples, and the compensation means applying the compensation term $e^{jkT_S\Delta\nu/2}$ when performing the correlation. From the numerical results one can see that the frequency error compensation is absolutely necessary. Furthermore, it is found that the accumulated time offset and Doppler effect have negligible impact on the TDOA estimation.

VII. Conclusions

In this paper, we have proposed the interferometry based sensing scheme for ISAC, by reusing communication signals and infrastructures. The principle of interferometry has been leveraged for improving the spatial resolution. The synchronization error in different antennas has been compensated, by using autofocus and compensation algorithms. Numerical simulations have demonstrated the validity of the proposed algorithms. One can see that the proposed algorithms can effectively reduce the impacts of timing and clock errors on the estimation, which lays the foundation for the implementation of the proposed interferometry scheme in existing cellular communication infrastructures. The future work in this direction includes 1) comparison with typical AOA estimation, 2) analysis of Doppler and multi-path effects, 3) consideration of multi-target scenario, and 4) extension to near-field regime.

References

[1] A. Liu, Z. Huang, and M. L. et al, "A survey on fundamental limits of integrated sensing and communication," *arxiv*, 2021.

[2] N. J. Willis, *Bistatic radar*. SciTech Publishing, 2005, vol. 2.

[3] K. Qian, C. Wu, Z. Yang, Y. Liu, and K. Jamieson, "Widar: Decimeter-level passive tracking via velocity monitoring with commodity wi-fi," in *Proc. of ACM Mobihoc*, 2017.

[4] X. Guo, B. Liu, C. Shi, H. Liu, Y. Chen, and M. C. Chuah, "Wifi-enabled smart human dynamics monitoring," in *Proc. of the 15th ACM Conference on Embedded Networked Sensor Systems (SenSys 2017)*, 2017.

[5] G. T. 38.857, "Study on nr positioning enhancements," ., 2020.

[6] Q. Inc., "What key technology inventions will drive the 5G expansion?" 2020. [Online]. Available: https://www.qualcomm.com/news/onq/2020/07/03/what-key-technology-inventions-will-drive-5g-expansion

[7] T. E. H. T. Collaboration, "First m87 event horizon telescope results. i. the shadow of the supermassive black hole," *The Astrophysical Journal Letters*, 2019.

[8] A. R. Thompson, J. M. Moran, and G. W. S. Jr., *Interferometry and Synthesis in Radio Astronomy, 3rd edition*. Springer, 2017.

[9] H. Li, N. Guo, and A. MacKenzie, "Interferometry based radar imaging by leveraging cellular communication networks," *preprint*, 2021.

[10] F. Lemic, J. Martin, C. Yarp, D. Chan, V. Handziski, R. Brodersen, G. Fettweis, A. Wolisz, and J. Wawrzynek, "Localization as a feature of mmwave communication," in *2016 International Wireless Communications and Mobile Computing Conference (IWCMC)*. IEEE, 2016, pp. 1033–1038.

[11] M. Alloulah and H. Huang, "Future millimeter-wave indoor systems: A blueprint for joint communication and sensing," *Computer*, vol. 52, no. 7, pp. 16–24, 2019.

[12] T. Wei and X. Zhang, "mtrack: High-precision passive tracking using millimeter wave radios," in *Proceedings of the 21st Annual International Conference on Mobile Computing and Networking*, 2015, pp. 117–129.

[13] S. Prasad M, T. Panigrahi, and M. Hassan, "Direction of arrival and center frequency estimation for impulse radio millimeter wave communications," in *Proceedings of the 2nd ACM Workshop on Millimeter Wave Networks and Sensing Systems*, 2018, pp. 63–68.

[14] M. Malanowski, *Signal Processing for Passive Bistatic Radar*. Artech, 2019.

[15] M. Radmard, M. Bastani, F. Behnia, and M. Nayebi, "Advantages of the dvb-t signal for passive radar applications," in *11-th INTERNATIONAL RADAR SYMPOSIUM*. IEEE, 2010, pp. 1–5.

[16] E. Glennon, A. Dempster, and C. Rizos, "Feasibility of air target detection using gps as a bistatic radar," *Positioning*, vol. 1, no. 10, 2006.

[17] A. Evers and J. A. Jackson, "Analysis of an lte waveform for radar applications," in *2014 IEEE Radar Conference*. IEEE, 2014, pp. 0200–0205.

[18] F. Wagner, F. Schiffers, F. Willomitzer, O. Cossairt, and A. Velten, "Intensity interferometry-based 3d imaging," *Optics Express*, vol. 29, no. 4, pp. 4733–4745, 2021.

[19] J. E. Baldwin and C. A. Haniff, "The application of interferometry to optical astronomical imaging," *Philosophical Transactions of the Royal Society A*, vol. 360, no. 174, 2002.

[20] Y. Wu, S. Rhodes, and E. H. Satorius, "Direction of arrival estimation via extended phase interferometry," *IEEE Trans. on Aerospace and Electronic Systems*, vol. 31, no. 1, pp. 375–381, 1993.

[21] "CPRI Specification V7.0."

[22] A. De la Oliva, J. A. Hernandez, D. Larrabeiti, and A. Azcorra, "An overview of the cpri specification and its application to c-ran-based lte scenarios," *IEEE Communications Magazine*, vol. 54, no. 2, pp. 152–159, 2016.

[23] C. Clivati, R. Aiello, G. Bianco, C. Bortolotti, P. De Natale, V. Di Sarno, P. Maddaloni, G. Maccaferri, A. Mura, M. Negusini *et al.*, "Common-clock very long baseline interferometry using a coherent optical fiber link," *Optica*, vol. 7, no. 8, pp. 1031–1037, 2020.

[24] R. Julie, T. Abbott, J. Burger, and R. Siebrits, "A novel high resolution optical time delay cable measurement system utilized in fiber verification in radio interferometry," in *2018 IEEE International Frequency Control Symposium (IFCS)*. IEEE, 2018, pp. 1–4.

[25] X. Niu, K. Yan, T. Zhang, Q. Zhang, H. Zhang, and J. Liu, "Quality evaluation of the pulse per second (PPS) signals from commercial GNSS receivers," *GPS solutions*, vol. 19, no. 1, pp. 141–150, 2015.